



ELSEVIER

Contents lists available at ScienceDirect

Electrochimica Acta

journal homepage: www.elsevier.com/locate/electactaInvestigation of electrochemical reduction of GeO₂ to Ge in molten CaCl₂-NaClLiangbin Rong^a, Rui He^a, Zhiyong Wang^a, Junjun Peng^a, Xianbo Jin^{a,*}, George Z. Chen^{a,b}^a College of Chemistry and Molecular Sciences, Wuhan University, Wuhan, 430072, PR China^b Department of Chemical and Environmental Engineering, and Energy and Sustainability Research Division, Faculty of Engineering, University of Nottingham, Nottingham, NG7 2RD, UK

ARTICLE INFO

Article history:

Received 18 May 2014

Received in revised form 17 September 2014

Accepted 22 September 2014

Available online 28 September 2014

Keywords:

Solid state reduction

Calcium germanates

GeO₂

Ge

Molten salt

ABSTRACT

Electrochemical reduction of solid GeO₂ has been investigated in the mixed CaCl₂-NaCl melt at 1023 K for developing a more efficient process for preparation of Ge. Cyclic voltammetry and potentiostatic electrolysis were applied to study the GeO₂-loaded metallic cavity electrode. In addition, porous GeO₂ pellets were reduced by potentiostatic and constant cell voltage electrolysis with a graphite anode, and the electrolysis products were analyzed by powder X-ray diffraction, scanning electron microscopy and energy-dispersive X-ray spectrometry, focusing on understanding the reduction mechanism and the impact of electrode potential on the product purity. It was found that the reduction of GeO₂ to Ge occurred at a potential of about -0.50 V (vs. Ag/Ag⁺), but generating various calcium germanates simultaneously, whose reduction was a little more difficult and needed a potential more negative than -1.00 V. However, if the cathode potential exceeded -1.60 V, Ca (or Na) - Ge intermetallic compounds might form. These results gave an appropriate potential range between -1.10 and -1.40 V for the production of pure germanium. Rapid electrolysis of GeO₂ to pure Ge has been realized at a cell voltage of 2.5 V with a current efficiency of about 92%.

© 2014 Elsevier Ltd. All rights reserved.

1. Introduction

Germanium (Ge) has attracted much attention for its electronic and optoelectronic applications as semiconductors and infrared optical components because of its larger excitonic Bohr radius and higher electron and hole mobility than Si. [1–3] Besides, the development of preparative techniques today allow more flexibility in manufacturing nanostructured germanium and its alloys [4–7], which are applied in negative electrode materials for lithium-ion batteries, optics fibers for long-distance communication applications, solar cells, catalysts and so on [8–11].

The conventional processes for preparation of Ge involve using the tannic acid to extract germanium concentrate from the minerals and then thermally reducing the obtained germanium oxides or sulfides to the pure metal by hydrogen or carbon. However, the volatile intermediate GeO or GeS species in these thermal processes might lead to elemental loss and environmental issues [12].

Electro-reduction of solid oxides on the cathode in molten salts at temperatures below 1173 K has attracted extensive attention in production of metals and alloys, and some progresses have been reviewed recently [13–15]. In particular, preparation of Si from SiO₂ by has been reported, and nanostructured Si can be successfully achieved [16–24]. Because Ge and Si have similar properties, the same technique may be utilized to obtain Ge nanowires [25]. However, the kinetics of the electro-reduction process and methods for elimination of some or all possible impurities should be likewise investigated.

The purpose of this work is to illustrate the mechanism of electro-reduction of solid GeO₂ to Ge in mixed CaCl₂-NaCl melt at 1023 K. Cyclic voltammetry and potentiostatic electrolysis as well as constant cell voltage electrolysis of the GeO₂ loaded metallic (Mo) cavity electrode (MCE) and GeO₂ pellets were implemented, intending to elaborate the influence of the cathode potential on purity of the Ge product.

2. Experimental

Anhydrous CaCl₂ (600 g, purity: >96 wt%, content of Mg and alkali metals: ~ 0.3 wt%) and NaCl (291 g) were mixed at

* Corresponding author. Tel.: +86 27 68756319; fax: +86 27 68756319.

E-mail address: xbjin@whu.edu.cn (X. Jin).

equi-molar ratio and dried at 573 K before melting at 1023 K in a graphite crucible placed in a stainless steel reactor under argon protection. Pre-electrolysis was performed at 2.6 V for 10 h to remove redox-active impurities (such as Mg and Zn) in the molten salt between a nickel foil cathode and a graphite rod anode.

Cyclic voltammograms (CVs) and potentiostatic electrolysis of solid GeO_2 in mixed CaCl_2 - NaCl melt were recorded using the metallic (Mo) cavity electrode (MCE) and a computer-assisted IVIUM Electrochemical System (Ivium Technologies BV Company). A small amount of GeO_2 powder (>99.999%, Nonfemet, Zhongjin Lingnan Shaoguan Smelter) was manually loaded into the double-cavity of the MCE (the inset in Fig. 1), which was then inserted into the molten salt as working electrode. The graphite counter electrode and an Ag/Ag^+ reference electrode (10 mol% AgCl , 45 mol% NaCl and 45% mol% KCl , sealed in a ceramic tube) were engaged in the electrochemical experiments.

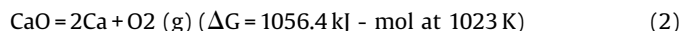
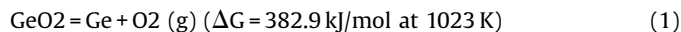
For potentiostatic electrolysis and two-electrode constant cell voltage electrolysis, the GeO_2 powder was pressed (8 MPa) into cylindrical porous pellets (~13.3 mm in diameter, ca. 1.4 mm in thickness, 0.6 g in mass, ~49% in porosity), which was then dried and sandwiched between two nickel foam sheets to form assembled cathodes. After being electrolyzed for 4 h at several potentials (-0.80 ~ -1.70 V) or constant cell voltage (2.5 V) controlled by a high accuracy battery tester (Shenzhen Neware Electronic Ltd. China), the pellets were lifted and cooled above the molten salt before being washed in distilled water and 0.5 mol/L HCl. The fine collected products were then dried and characterized by an X-ray diffraction (SHIMADZU Lab XRD-6000 with $\text{Cu K}\alpha 1$, scanning rate of $6^\circ/\text{min}$), scanning electron microscopy (FEI Sirion Field Emission Gun SEM system) together with energy-dispersive X-ray analysis (EDX), and transmission electron microscopy (JEM-2100, JEOL Ltd.). The oxygen content was determined by inert gas fusion oxygen analysis (RO-416DR, LECO, USA).

3. Results and discussion

Fig. 1A presents the consecutive CVs of MCE- GeO_2 electrode in the mixed CaCl_2 - NaCl melt at 1023 K. The CV of the blank MCE (dash line) revealed that the electro-reduction of $\text{Ca}^{2+}/\text{Na}^+$ and redissolution of Na/Ca took place at potentials around -2.30 V near the negative scan limit. Thermodynamically, the formation of Na and Ca could occur at adjacent potentials considering the theoretical decomposition voltages of CaCl_2 and NaCl are 3.326 and 3.284 V at 1023 K respectively. Compared with the blank, the CVs of MCE- GeO_2 exhibited mainly five reduction steps in the first cycle, showing an onset potential of around -0.50 V (solid line). In the subsequent cycles, the broad reduction peaks C0 disappeared. The small but notable peaks at potential about

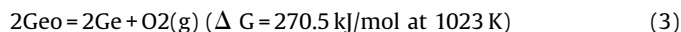
-0.80 V can be regarded as reduction coupled with the anodic peak A0. While other cathodic and anodic peaks remained distinct, CVs within different potential ranges were recorded to recognize the redox pairs. As Fig. 1B indicates definitely C1 and A1 to be redox pair, a comparison between Fig. 1A and C suggests that C2/A2, C3/A3 and C4/A4 are redox couples respectively.

Thermodynamic calculations were carried out to help understand the reduction of GeO_2 ,



According to Reactions (1) and (2), the theoretical decomposition voltages of GeO_2 and CaO at 1023 K are 0.992 and 2.737 V respectively. The difference between the two suggesting that the reduction of GeO_2 to Ge could occur at a potential at least 1.745 V more positive than that of Ca formation, which happens at potentials around -2.30 V as shown in Fig. 1A. Thus, peak C0 in Fig. 1A with an onset potential of -0.50 V is most likely due to the reduction of GeO_2 to Ge.

Both peak currents of C1 and A1 (shown in Fig. 1A) decreased along with the increasing the number of cycles. Based on previous studies [26], it was deemed that oxygen ionization showed irreversibility on continuously recorded CVs due to the irreversible migration of oxygen ions from the solid cathode to the molten salt. Also, in a single cycle the cathodic current always exceeded the anodic one, indicating the irrecoverable loss of oxygen ions which are needed for the re-oxidation. Therefore, C1 can be ascribed to another oxygen ionization process in addition to C0. Ge has a divalent oxide GeO which however could not be the intermediate product for C1 taking the below thermodynamic calculation into account,



It can be found from Reactions (1) and (3) that the reduction of GeO would happen at a potential 291 mV more positive than GeO_2 , thus, GeO should be electrochemically unstable at the reduction potentials of GeO_2 (-0.50 V or more negative). Since its onset potential was as negative as -1.05 V, peak C1 was suggested to be the reduction of calcium germanates as will be discussed later in detail.

Redox couples C2/A2 and C3/A3 were highly reversible in comparison with C1/A1. Their cathodic and anodic currents increased successively in the initial cycles. These reduction currents were unlikely to be due to the oxygen ionization processes. It was thus thought that all the GeO_2 could have been reduced to metallic Ge in the potential region of C1. To verify this

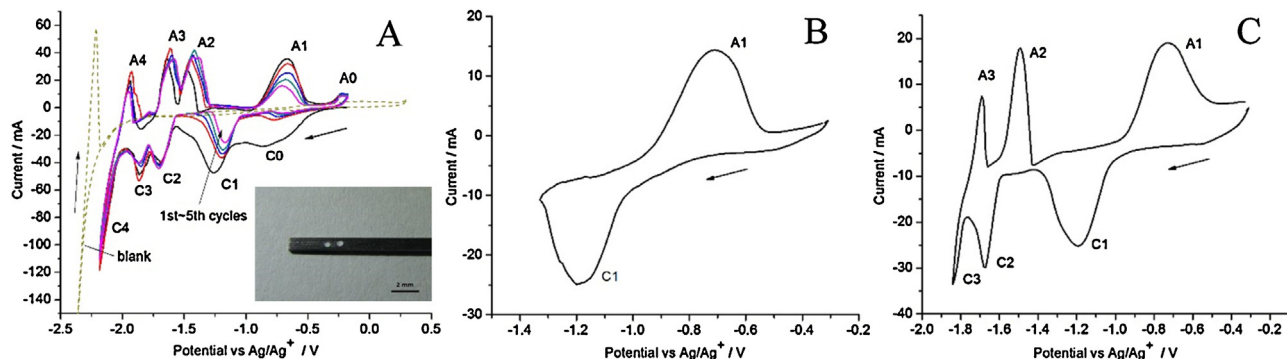


Fig. 1. (A) Cyclic voltammogram (CV) of the blank MCE (dashed line) and consecutive CVs of the GeO_2 powder loaded MCE. The inset image shows the metallic (Mo) cavity electrode (MCE). (B) and (C), the second cycle CV of the GeO_2 powder loaded MCE in ranges of -0.3 ~ -1.35 and -0.3 ~ -1.95 V respectively. All CVs were recorded in the mixed CaCl_2 - NaCl melt at 1023 K and $50 \text{ mV}\cdot\text{s}^{-1}$.

assumption, potentiostatic electrolysis of MCE-GeO₂ electrodes was carried out at -1.40 V (vs. Ag/Ag⁺) for several periods of time and the electro-reduction products in the cavities were investigated by SEM and EDX after washing in distilled water.

As shown in Fig. 2A, the original particles of the loaded GeO₂ in the MCE were about 10 μm in sizes with aggregated granules. After only 5 s electrolysis at -1.40 V, the morphology changed greatly to a mixture of nanoparticles and nanofibers. The oxygen content decreased to about 4.9 wt. %, suggesting removal of about 88% of O. The nanofibers in the 15 s electrolytic product became wider and shorter, and the oxygen content was about 2.9 wt. %. EDX analysis showed the existence of Ca element in these products. Formation of calcium metallates happened quite often during the electrolysis of many other metal oxides [14]. These nanofibers disappeared in the 60 s product, which was confirmed to be pure Ge consisting of predominantly nanoparticles by the SEM and EDX analyses. These results confirmed that peak C1 was the reduction of any intermediates to Ge.

Peaks C2 to C4 were then suggested to be the formation of the Ca (or Na)-Ge intermetallic compounds. The successive increase of their currents in the early potential cycles could be linked to the gradual reduction of GeO₂ to Ge until completion. As can be seen from the Ca-Ge and Na-Ge binary phase diagrams [27] (Fig. 3), many compounds such as Ge₄Na, GeNa, GeNa₃, Ge₂Ca, GeCa, GeCa₂ might form during the cathodic polarization of Ge. Thus, proper reduction potentials of GeO₂ should be determined to avoid the formation of these intermetallic compounds, which will be focused in the following discussion.

According to the above analyses and discussion of the CVs of the MCE-GeO₂, potentiostatic electrolysis of GeO₂ pellets were conducted at several potentials ranging from -0.80 to -1.70 V for 4 h to further understand the steps in the reduction of GeO₂.

Typical current-time plots are shown in Fig. 4A. At -0.80 V (before peak C1), it can be seen that the GeO₂ underwent a small cathodic current (40~300 mA) passed through the oxide pellet with a reduction charge of about 1000 C after taking away the background. This corresponds to only partial reduction of the 0.6 g pellet because the theoretical charge needed for the complete reduction is about 2210 C. However, peaks of GeO₂ disappeared on the XRD pattern (Fig. 4B), which showed a mixture of Ge and calcium germanates (CaGeO₃, CaGe₄O₉, and Ca₃GeO₅). The SEM image of the -0.80 V product after washing in water is presented in Fig. 5A, which reveals nanofibers and nanoparticles similar to those in Fig. 2B and 2C. The existence of calcium germanates in the -0.80 V product was confirmed by the inserted EDX spectrum in Fig. 5A. Since calcium germanates can dissolve into hydrochloric acid but germanium will not, the -0.80 V product was further washed in the 0.5 mol/L HCl solution. It was found that most of the nanofibers were dissolved, and the remaining products were mainly Ge particles as revealed by the SEM and EDX analyses shown in Fig. 5B.

At -1.1 V, the initial reduction current increased to about 3 A (Fig. 4A), and then leveled off in about 20 min, suggesting a very fast step. Then the current decreased slowly in the rest of the electrolysis time, and the reduction charge reached about 2200 C in the 4-h electrolysis. Both the XRD (Fig. 4B) and EDX analyses (Fig. 5C) suggested that all the electrolytic products at potentials ranging from -1.10 to -1.40 V were pure Ge, indicating that the GeO₂ and calcium germanates could be reduced to Ge at these potentials. In addition, during washing these samples in water, no gas bubbles were observed, indicating no Ca-Ge or Na-Ge compounds formed at these potentials. The Ge samples were principally composed of Ge nanoparticles with primary particle sizes of about 100 nm (Fig. 5C). It should be pointed out that the morphology of the

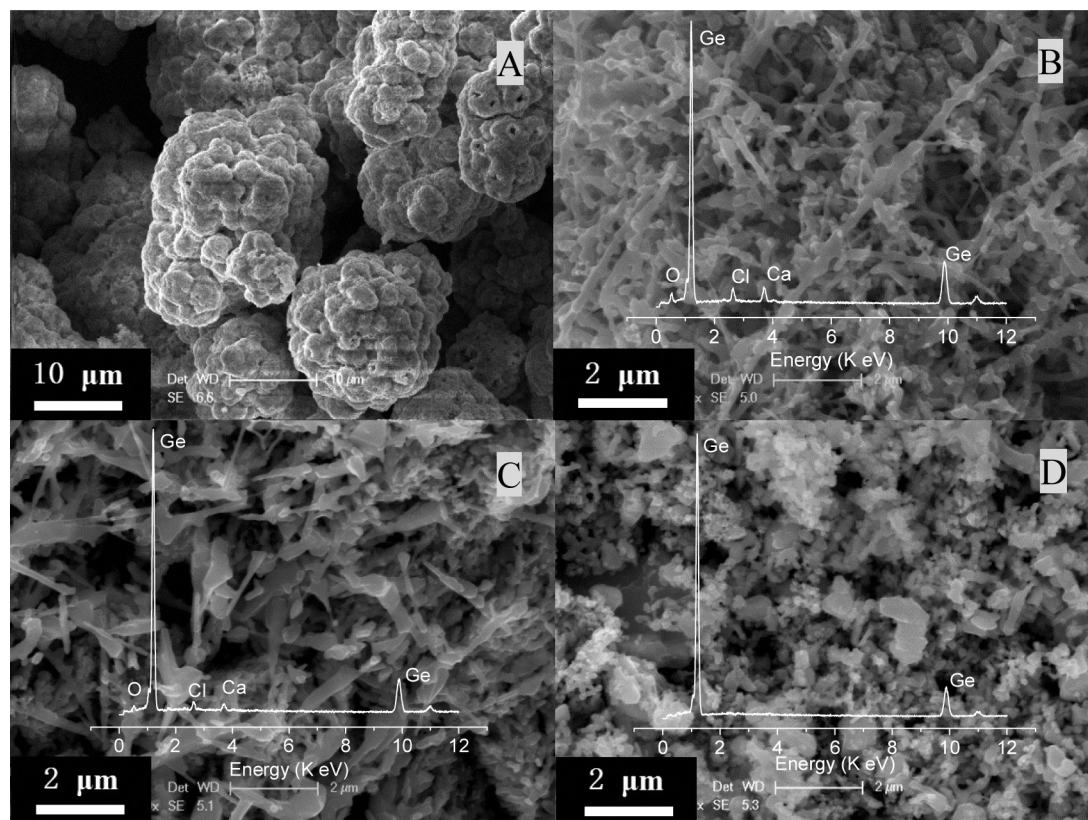


Fig. 2. The SEM images of the products from potentiostatic electrolysis of the GeO₂ powder loaded MCE in the CaCl₂-NaCl melt at -1.4 V (vs. Ag/Ag⁺) and 1023 K for different times: (A) 0 s; (B) 5 s; (C) 15 s; (D) 60 s. The insets show the respective EDX spectra.

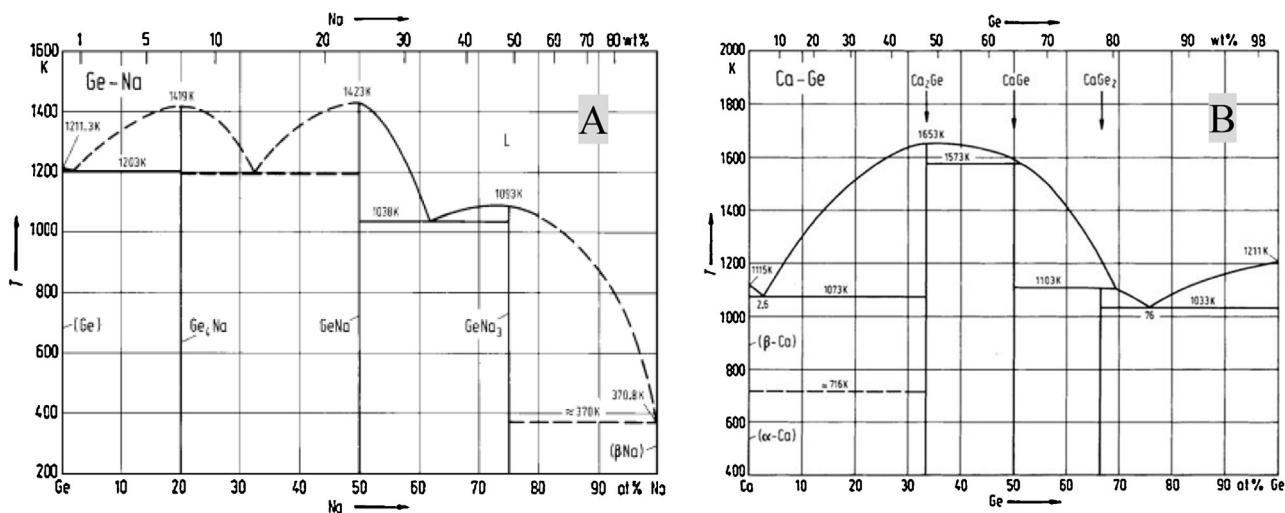


Fig. 3. The Na-Ge (A) and Ca-Ge (B) binary phase diagrams [27].

metallic Ge generated in this work at 1023 K was in great differences from that prepared by electrolysis of GeO₂ at 873 K in the equi-molar CaCl₂-NaCl melt, which was reported to be consisting of mainly nanowires [25]. Similarly, depending on the electrolysis conditions, either nanoparticles or nanowires of Si could be prepared by electrolysis of solid SiO₂ in the CaCl₂ based melts [16–24]. It was found that Si nanowires would become dominant in the product upon electrolysis of porous pellet of SiO₂ particularly with nanoparticles of the oxide [22], addition of nanoparticles of Au as catalyst [23], and/or application of a low overpotential for slow reduction [24]. While other conditions were likely very similar, it may be speculated that the morphology difference in the Ge products from these two temperatures was mainly due to the difference in the reduction speed of the solid cathode (4 h for 0.6 g GeO₂ in this work vs. ~12 h at 873 K for 0.5 g GeO₂ in the previous work [25]). Generally, a slower reduction speed is more favorable for formation of fewer nuclei and oriented growth of crystals.

Ge and Si are both in the C group (or group 14) of the Periodical Table, and can form various intermetallic compounds with Ca and Na. An optimized potential range for the preparation of pure Si has been suggested [28]. To prepare pure Ge from GeO₂ with minimum contamination of Ca (or Na), the upper limit potential needs to be

determined. As shown in Fig. 4A, the initial reduction current at -1.7 V was much greater than that at -1.1 V, obviously due to the increased overpotential. However, after that, another current plateau between 20 and 90 min could be observed. At the same time, the total cathodic charge increased to about 3700 C, which was far beyond that needed theoretically for the reduction of GeO₂ to Ge. As revealed by XRD (Fig. 4B), the direct electrolysis product at -1.70 V before any washing contained mainly Ca_{0.33}Ge and some salts from the CaCl₂-NaCl melt. Some CaO as the existing form of the generated O²⁻ ions in the melt could also be found [29]. The Ca_{0.33}Ge phase matched up with the eutectoid containing 76 at. % of Ge in the Ge-Ca phase diagram (Fig. 3B). During washing in water, reaction between the Ca_{0.33}Ge and water occurred as evidenced by the generation of gas bubbles, leading to an amorphous product containing Ca, Ge and O as revealed by the SEM and EDX analyses in Fig. 5D. These results suggested again that peak C2 on the CVs in Fig. 1 corresponded to the formation of Ca-Ge intermetallic compounds, thus the potential for the electro-reduction of GeO₂ to pure Ge should be controlled in a range between -1.00 V and -1.40 V.

According to the above discussion, the mechanism of the reduction of GeO₂ to Ge during electrolysis of the solid GeO₂ in the CaCl₂-NaCl melt was suggested as below,

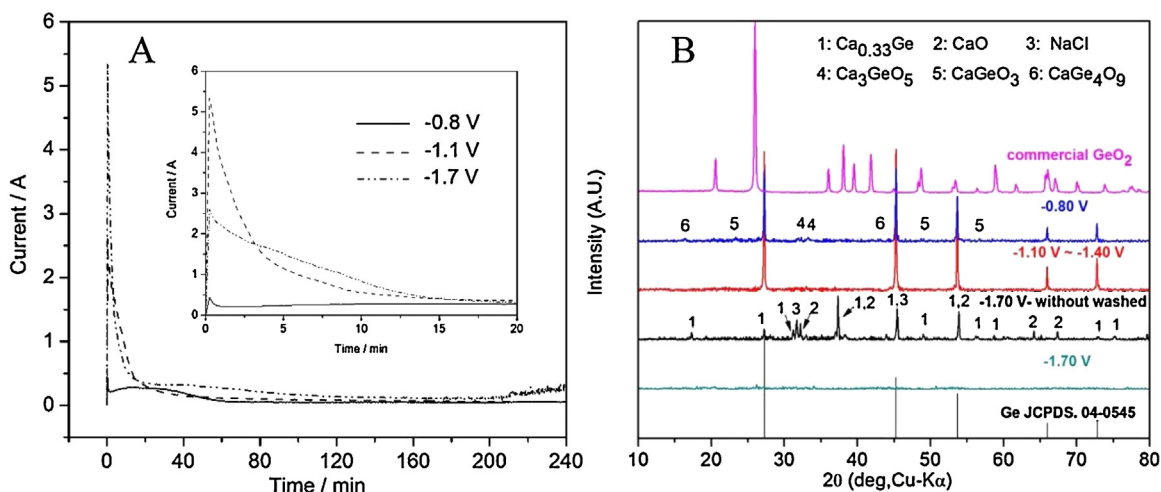


Fig. 4. (A) Typical current-time curves recorded during the potentiostatic electrolysis of GeO₂ pellets (ca. 0.6 g) in the CaCl₂-NaCl melt at the indicated potentials (vs. Ag/Ag⁺) and 1023 K for 4 h; (B) XRD patterns of GeO₂ and the 4-hour electrolysis products obtained at the indicated potentials. All the samples were washed in water if not specified.

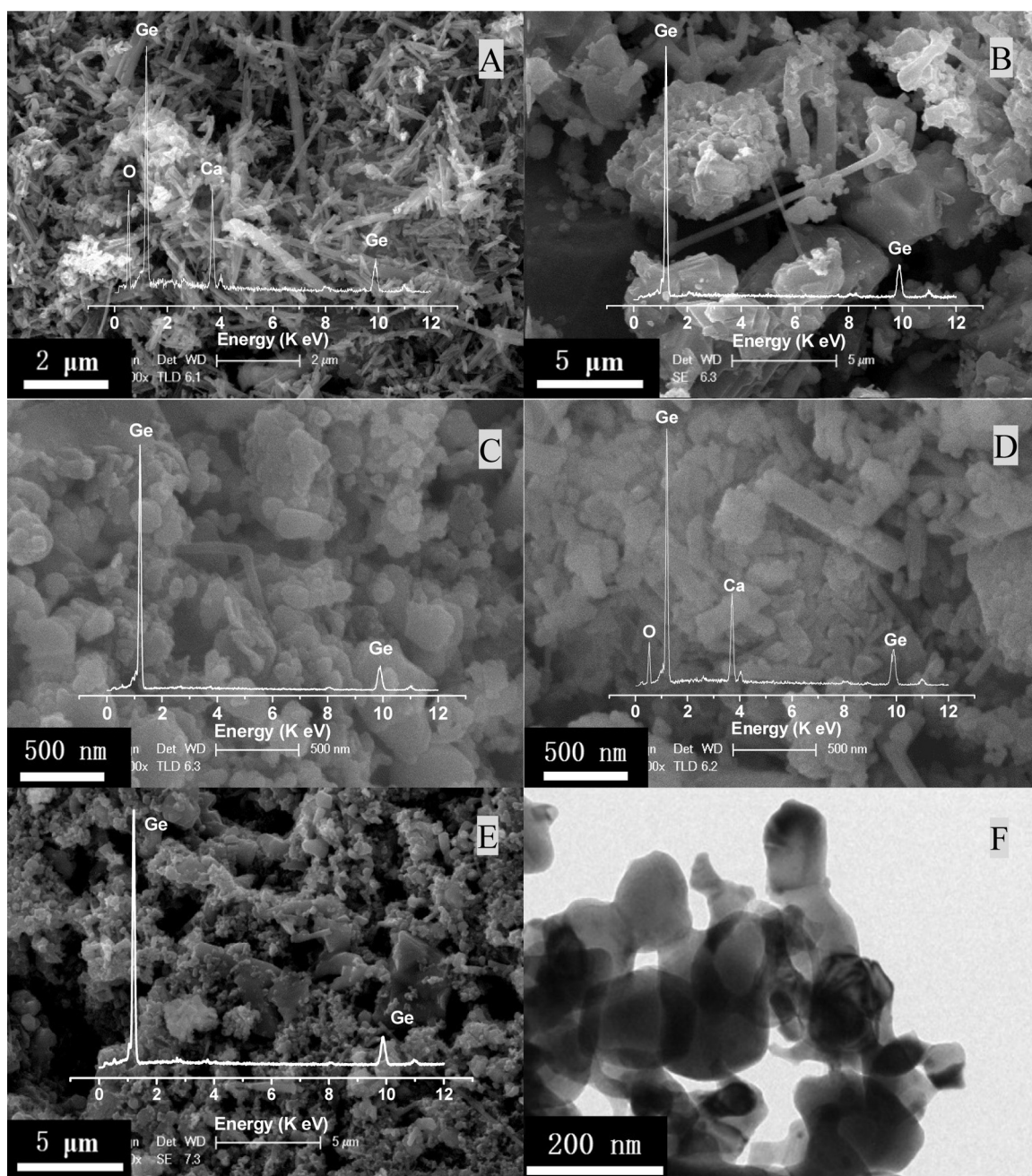
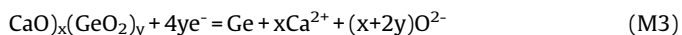
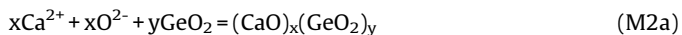


Fig. 5. SEM images of the products from the potentiostatic electrolysis of porous GeO_2 pellets in the CaCl_2 - NaCl melt for 4 h at 1023 K and different potentials (vs. Ag/Ag^+): (A) and (B), -0.80 V; (C), -1.40 V; (D) -1.70 V. And the SEM (E) and TEM (F) images of the electrolysis product of a GeO_2 pellet at cell voltage of 2.5 V for 4 h. The insets show the corresponding EDX spectrums. The samples were washed in distilled water except for (B), which was observed after washing in HCl solution.



The O^{2-} ions generated from Reaction M1 and M3 could be dissociative if in low concentration (Reaction M2a) or CaO

precipitation upon saturation (Reaction M2b). It is worth noting that formation of Ca-M-O (M = the studied metal, such as Ti, Zr, Hf, Cr, Ta, Nb) metallates during electrolysis of various metal oxides have been reported previously [31–39]. One suggested mechanism of formation of the composite oxide was the electrochemical insertion of Ca^{2+} into the metal oxide, usually resulting in a partial reduction in case that the valence of the metal element (such as Ti) may vary continuously [31]. Since the valence of Ge in the calcium germanates is basically +4, the reaction between the unreduced GeO_2 , the O^{2-} generated from reaction M1 and Ca^{2+} from the melt was suggested to be responsible for the formation of calcium germanates in this work (Reaction M2), which was supported by the following thermodynamic calculation taking CaGeO_3 as an example,

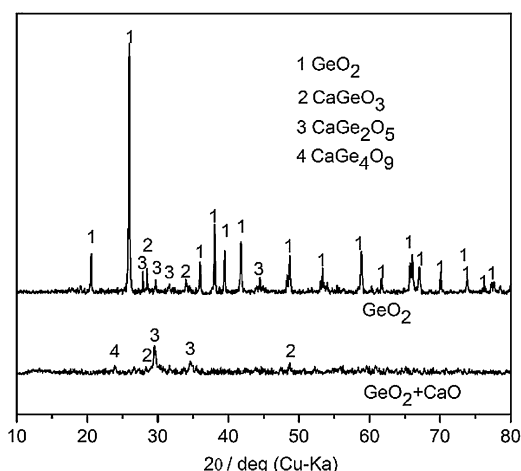


Fig. 6. XRD patterns of GeO_2 and GeO_2+CaO after immersion of their pellets in $\text{CaCl}_2\text{-NaCl}$ melt at 1023 K for 2 h.



Reaction (4) indicates that the formation of CaGeO_3 should be spontaneous at the studied temperature. However, if combining Reaction (M1) and (M2a), and also taking CaGeO_3 as an example, there is,



Reaction (5) could indicate another mechanism for the formation of Ca-M-O composites by redistribution of the O in the solid state [37–39]. Theoretically, if one considers that the origin of CaO in Reaction (4) results from the reduction of GeO_2 via Reaction (M1) in molten CaCl_2 , there is no thermodynamic difference for CaGeO_3 to be formed via either Reaction (4) or (5), and it is also difficult to distinguish them experimentally. Nevertheless, the feasibility of Reaction (4) has been verified by a direct reaction between GeO_2 and CaO in the $\text{CaCl}_2\text{-NaCl}$ melt at 1023 K. As shown in Fig. 6, after immersion of a CaO + GeO_2 (1:1 in molar ratio) pellet in the melt for about 2 h, the originally strong XRD peaks of GeO_2 disappeared. Instead, the XRD pattern showed a mixture of various germanates, in accordance with the multiphase equilibrium feature of a CaO– GeO_2 system [40]. In contrast, after immersion of a pure GeO_2 pellet in the melt, the resultant was still GeO_2 as revealed by XRD analysis shown in Fig. 6. A few amount of calcium germanates did have formed, which is thought to be due to

the reaction between the GeO_2 and the CaO impurity due to the hydrolysis of CaCl_2 . Slight dissolution of GeO_2 could not be excluded, however, the solubility of GeO_2 in the melt should be very low considering that the pellet maintained its original shape perfectly after the 2-hour immersion.

It is claimed previously that no experimental proof of formation of germanates as the intermediate products during electrolysis of the GeO_2 pellets in the $\text{CaCl}_2\text{-NaCl}$ melt at the 873 K [25]. However, some small but remarkable XRD peaks of the electrolysis products that might be evidences of calcium germanates have been overlooked, and no elemental analysis of the partially reduced samples has been carried out. In this work, it was found that the XRD peaks of the calcium germanates were much weaker than those of GeO_2 and Ge, although their content could be significant according to the EDX analysis.

Constant cell voltage electrolysis of GeO_2 pellets to mimic a traditional two-electrolysis process was also studied at a cell voltage of 2.5 V. This voltage was selected according to the above results of CV and potentiostatic electrolysis considering that it should be significantly lower than the decomposition voltage of the melt (about 3.3 V) to avoid the formation of Ca-Ge or Na-Ge compounds, but should be sufficiently high to ensure a relatively fast electrolysis by overcoming the possible ohmic and concentration polarizations in the assembled cell. It should be pointed out that besides the electrolysis current, the cell voltage should be also highly dependent on the cell configuration. In this study, the 0.6 g GeO_2 pellets (1.33 cm in diameter) were electrolyzed against a graphite rod (1.8 cm in diameter) with about 3 cm immersed into the melt, and the distance between the cathode and anode was about 3 cm.

The typical current-time plot recorded during the electrolysis process was presented in Fig. 7A. As shown in the enlarged insert, the current responding to the suddenly imposed 2.5 V voltage shows charging of double layer at initial, after which the reduction current climbed then decreased forming a reduction current peak as commonly observed in previous electrolysis of various solid oxides [41,42], which has been rationalized by the dynamic metal/metal oxide/electrolyte three phase electrochemical interline (3PI) theories [30]. In brief, the electro-reduction took place initially at the current collector (foam nickel)/metal oxide (GeO_2)/electrolyte (molten salts) three phase interlines. Although the electronic contact between the Ni and the pellet might be limited, the reduction generated porous metal, the conjunctive unreduced oxide and the electrolyte in the pores of the electrode could

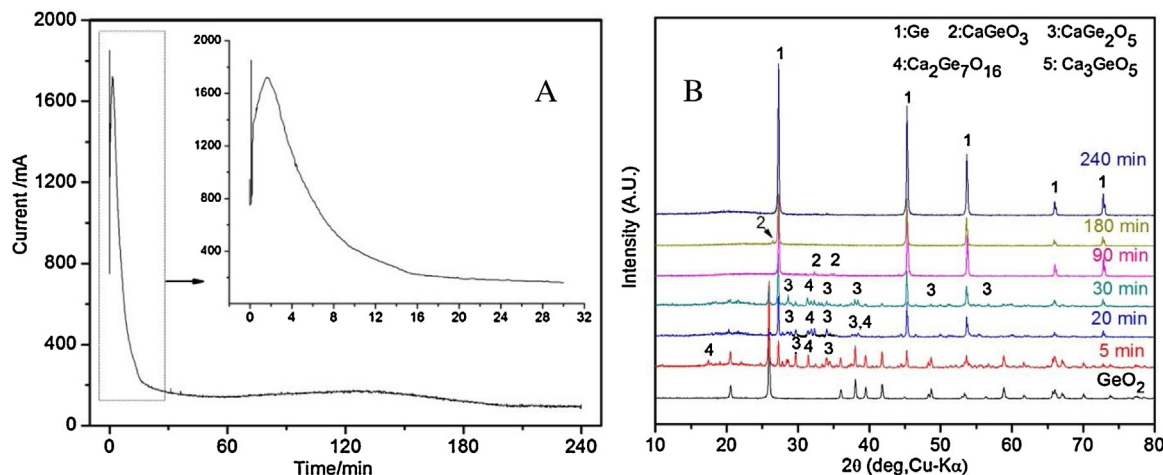


Fig. 7. (A) Current-time plot recorded during potentiostatic electrolysis of the GeO_2 pellet at a cell voltage of 2.5 V. (B) XRD patterns of electrolytic samples obtained from different stages of electrolysis.

construct the new 3PIs. The transverse expansion of such 3PIs on the pellet surface caused the initial increase of the cathodic current, which then decreased due to the increasing ohmic and mass transfer polarization of the reduction in the depth direction.

The total electrolytic current–time curve of the 2.5 V electrolysis showed basically two reduction steps (Fig. 7A). The first one was very quick as reflected by the large current with a maximum of around 1700 mA, which declined to about 200 mA in about 20 min. The following platform current with some slight fluctuations lasted about 200 min suggesting a relatively slower second reduction step. To make a good understanding, the reduction products generated at different stages of electrolysis were characterized by XRD. It can be seen from Fig. 7B that the electrolysis impelled the gradual decrease of intensity of the XRD peaks of GeO₂, which disappeared in about 30 min. As expected, accompanying with the formation of Ge, various calcium germanates (CaGeO₃, Ca₃GeO₅, CaGe₂O₅ and Ca₂Ge₇O₁₆) emerged immediately after imposing the 2.5 V voltage. The subsequent reduction of germanates were much tardy. Even after 180-min electrolysis, diffraction peaks of CaGeO₃ were still perceivable in the XRD pattern of the product. This phenomenon was different from those report on the electrolysis of solid SiO₂, where CaSiO₃ was seldom found in a partially reduced sample [16–24]. However, the CaSiO₃ was stable only at the very beginning reduction potential of SiO₂, and could be reduced to Si at a slightly larger overpotential [21,24].

The results from the constant cell voltage electrolysis at 2.5 V were in well agreement with the above suggested reduction mechanism (reactions M1 to M3). In addition, it was demonstrated that the reduction of calcium germanates to Ge may be the rate determining step for the complete reduction of a GeO₂ pellet. Nevertheless, the 4-hour electrolysis has led to a full reduction as confirmed by the EDX analysis shown in Fig. 5E, which displayed almost no any X-ray peak of other element but those of Ge, suggesting a content less than 0.5 wt. % (the limit of detection of EDX analysis) of any impurity.

The SEM in Fig. 5E suggests nodule morphology of the generated Ge powders, consisting of both micrometer and nanometer particles. The TEM inspection (Fig. 5F) revealed that the primary particle size of the nanometer particles was around 100 nm. The existence of large particles of Ge was thought to be due to the sintering of Ge at the electrolysis temperature (1023 K) considering that the melting point of Ge is only about 1211 K.

The mass of the metallic product from the 0.6 g GeO₂ pellet was about 0.4 g, indicating an elemental recovery of Ge of about 96.8%. The little loss might be mainly due to the difficulties in collecting Ge nanoparticles during the processing. It is speculated that unlike a traditional hydrogen thermo-reduction process where GeO would form and escape away, this electrolytic method can provide much stronger driven force for the reduction of any Ge containing species to Ge, thus higher yield could be achieved. The metallic product remained stable in air, and the oxygen content in the sample after shelving for about 6 months was determined by inert gas fusion oxygen analysis to be about 0.71 wt. %, which might mainly arise from the surface oxidation of the Ge nanoparticles.

According to the current–time plot shown in Fig. 7a, the actual charge passed for the reduction of 0.6 g GeO₂ to Ge (requires ~2210 C theoretically) during the 4-h electrolysis was about 2400 C, indicating a current efficiency of about 92%. This current efficiency was significantly higher than those reported for the electrolysis of other refractory metals, such as TiO₂ (15~32% for dense pellets and 54% for TiO₂ pellets with an optimized porosity) [43,44]. It has been recognized that the loss of current efficiency during the electrolysis could be mainly attributed to the generation of dissolved Ca at the cathode and the electronic conductivity of the molten salts [45,46]. However, for the

electrolysis of GeO₂ that could proceed quickly at -1.1 V, the dissolved Ca (about 10⁻¹² in activity) would be neglectable considering that the Ca with an activity of 1 would only form at about -2.3 V from Fig. 1. In addition, the low cell voltage and quick electrolysis speed were both helpful to achieve a high current efficiency. On the other hand, the discharge of O²⁻ ions at the graphite anode resulted in CO₂ emission and some carbonate that dissolved into the melt. The carbonate ions would move to the cathode and reduce to C with O²⁻ regenerated, which could also decrease the current efficiency and cause carbon contamination to the metallic product [33]. Fortunately, while the relatively low cell voltage for the GeO₂ electrolysis would somewhat suppress these shuttle reactions, the fact that Ge forms no any alloy with C would help to alleviate the carbon contamination during electrolysis and/or remove the carbon from the Ge product later, and it is worth noting that Ge has been produced by carbothermic reduction traditionally [12].

7. Conclusions

The direct electro-reduction of solid GeO₂ in the equimolar CaCl₂–NaCl melt was studied at 1023 K and pure Ge can be prepared at a potential range between -1.10 V and -1.40 V (vs. Ag/Ag⁺). Cyclic voltammetry, potentiostatic and constant cell voltage electrolysis together with XRD, EDX analyses and SEM observation suggested that the mechanism for the reduction of solid GeO₂ includes (1) electrochemical reduction of GeO₂ to Ge; (2) chemical formation of calcium germanates ((CaO)_x(GeO₂)_y) and (3) electrochemical reduction of (CaO)_x(GeO₂)_y to Ge. Although the first step can start at a potential (-0.5 V vs. Ag/Ag⁺) about 1.8 V more positive than that of cathodic decomposition of the electrolyte, the reduction released O²⁻ together with the Ca²⁺ from the electrolyte react immediately with remaining GeO₂, generating the germanates whose reduction occurs at potentials more negative than -1.0 V with a relatively slow speed. An increased polarization is expected to speed up the reduction of the germanates. However, potentials exceeding -1.60 V will lead to the formation of Ca–Ge or Na–Ge intermetallic compounds. Based on these understandings, rapid electrolysis of GeO₂ to pure Ge has been carried out at a cell voltage of 2.5 V. A current efficiency as high as 92% and an elemental recovery of about 96.8% were achieved. The electrolytic Ge exhibits a mixture of micrometer particles and sub-micrometer nodular particles with the primary particle sizes of around 100 nm. These findings promise a new approach for the metallurgy of GeO₂, as well as preparation of nanometer Ge powders.

Acknowledgements

This work is supported by NSFCs (21173161, 20973130), the 863 project (2009AA03Z503), the MOE Program (NCET-11-0397), the Fundamental Research Funds for the Central Universities, and the Large-scale Instrument and Equipment Sharing Foundation of Wuhan University.

References

- [1] J. Andzane, N. Petkov, A.I. Livshits, J.J. Boland, J.D. Holmes, D. Ertz, Two-Terminal Nanoelectromechanical Devices Based on Germanium Nanowires, *Nano Lett.* 9 (2009) 1824–1829.
- [2] L. Li, X. Fang, H.G. Chew, F. Zheng, T.H. Liew, X. Xu, Y. Zhang, S. Pan, G. Li, L. Zhang, Crystallinity-Controlled Germanium Nanowire Arrays: Potential Field Emitters, *Adv. Funct. Mater.* 18 (2008) 1080–1088.
- [3] R.P. Prasankumar, S. Choi, S.A. Trugman, S.T. Picraux, A.J. Taylor, Ultrafast Electron and Hole Dynamics in Germanium Nanowires, *Nano Lett.* 8 (2008) 1619–1624.
- [4] H.C. Wu, T.C. Hou, Y.L. Chueh, L.J. Chen, H.T. Chiu, C.Y. Lee, One-Dimensional Germanium Nanostructures-Formation and Their Electron Field Emission Properties, *Nanotechnology* 21 (2010) 455601.

- [5] V.Y. Aleshkin, A.A. Dubinov, Direct Band Ge and Ge/InGaAs Quantum Wells in GaAs, *J. Appl. Phys.* 109 (123) (2011) 107.
- [6] A. Alkhatib, A. Nayfeh, A Complete Physical Germanium-on-Silicon Quantum Dot Self-Assembly Process, *Sci. Rep.* 3 (2013) 2099.
- [7] S.K. Ray, R.K. Das, S. Manna, A. Dhar, Structural and Optical Properties of Germanium Nanostructures on Si(100) and Embedded in High-K Oxides, *Nanoscale Res. Lett.* 6 (2011) 224.
- [8] R. Pillarisetty, Academic and Industry Research Progress in Germanium Nanodevices, *Nature* 479 (2011) 324–328.
- [9] D.D. Vaughn 2nd, R.E. Schaak, Synthesis, Properties and Applications of Colloidal Germanium and Germanium-Based Nanomaterials, *Chem. Soc. Rev.* 42 (2013) 2861–2879.
- [10] M.H. Park, Y. Cho, K. Kim, J. Kim, M. Liu, J. Cho, Germanium Nanotubes Prepared by Using the Kirkendall Effect as Anodes for High-Rate Lithium Batteries, *Angew. Chem. Int. Ed. Engl.* 50 (2011) 9647–9650.
- [11] V. Soriano, L. Colace, C.M. Ragliano, D. Fulgoni, L. Nash, G. Assanto, Germanium-on-Glass Solar Cells Fabrication and Characterization, *Opt. Mater. Express* 3 (2013) 216–228.
- [12] R.R. Moskalyk, Review of Germanium Processing Worldwide, *Miner. Eng.* 17 (2004) 393–402.
- [13] G.Z. Chen, D.J. Fray, T.W. Farthing, Direct electrochemical reduction of titanium dioxide to titanium in molten calcium chloride, *Nature* 407 (2000) 361–364.
- [14] A.M. Abdelkader, K. Tripuraneni Kilby, A. Cox, D.J. Fray, DC Voltammetry of Electro-deoxidation of Solid Oxides, *Chem. Rev.* 113 (2013) 2863–2886.
- [15] W. Xiao, D. Wang, The Electrochemical Reduction Processes of Solid Compounds in High Temperature Molten Salts, *Chem. Soc. Rev.* 43 (2014) 3215–3228.
- [16] X. Jin, P. Gao, D. Wang, X. Hu, G.Z. Chen, Electrochemical Preparation of Silicon and Its Alloys from Solid Oxides in Molten Calcium Chloride, *Angew. Chem. Int. Ed.* 43 (2004) 733–736.
- [17] T. Nohira, K. Yasuda, Y. Ito, Pinpoint and Bulk Electrochemical Reduction of Insulating Silicon Dioxide to Silicon, *Nat. Mater.* 2 (2003) 397–401.
- [18] E. Ergül, I. Karakaya, M. Erdoğan, Electrochemical Decomposition of SiO₂ Pellets to Form Silicon in Molten Salts, *J. Alloys Compd.* 509 (2011) 899–903.
- [19] J. Zhao, J. Li, P. Ying, W. Zhang, L. Meng, C. Li, Facile Synthesis of Freestanding Si Nanowire Arrays by One-step Template-free Electro-deoxidation of SiO₂ in a Molten Salt, *Chem Commun.* 49 (2013) 4477–4479.
- [20] E. Juzeliunas, A. Cox, D.J. Fray, Electro-deoxidation of Thin Silica Layer in Molten Salt-globular Structures with Effective Light Absorbance, *Electrochim. Acta* 68 (2012) 123.
- [21] K. Yasuda, T. Nohira, R. Hagiwara, Y.H. Ogata, Diagrammatic Representation of Direct Electrolytic Reduction of SiO₂ in Molten CaCl₂, *J. Electrochem. Soc.* 154 (2007) E95.
- [22] J. Yang, S. Lu, S.X. Kan Zhang, J. Du, Electrochemical Preparation of Silicon Nanowires from Nanometre Silica in Molten Calcium Chloride, *Chem. Commun.* (2009) 3273–3275.
- [23] Y. Nishimura, T. Nohira, K. Kobayashi, R. Hagiwara, Formation of Si Nanowires by Direct Electrolytic Reduction of Porous SiO₂ Pellets in Molten CaCl₂, *J. Electrochem. Soc.* 158 (2011) E55.
- [24] W. Xiao, X. Jin, G.Z. Chen, Up-scalable and Controllable Electrolytic Production of Photo-responsive Nanostructured Silicon, *J. Mater. Chem. A* 1 (2013) 10243.
- [25] H. Yin, W. Xiao, X. Mao, W. Wei, H. Zhu, D. Wang, Template-free Electrosynthesis of Crystalline Germanium Nanowires from Solid Germanium Oxide in Molten CaCl₂-NaCl, *Electrochim. Acta* 102 (2013) 369–374.
- [26] H.P. Gao, X.B. Jin, S.W. Zou, F.Z. Ling, J.J. Peng, Z.Y. Wang, G.Z. Chen, Liquid Diffusion of the Instantaneously Released Oxygen Ion in the Electrolytic Porous Fe from Solid Fe₂O₃ in Molten CaCl₂, *Electrochim. Acta* 107 (2013) 261–268.
- [27] H. Landolt, R. Börnstein, Phase Equilibria Crystallographic and Thermodynamic Data of Binary Alloys, Springer-Verlag, 1993.
- [28] W. Xiao, X. Jin, Y. Deng, D. Wang, G.Z. Chen, Rationalisation and Optimisation of Solid State Electro-Reduction of SiO₂ to Si in Molten CaCl₂ in Accordance with Dynamic Three-Phase Interlines Based Voltammetry, *J. Electroanal. Chem.* 639 (2010) 130–140.
- [29] R. Bhagat, D. Dye, S.L. Raghunathan, R.J. Talling, D. Inman, B.K. Jackson, K.K. Rao, R.J. Dashwood, In Situ Synchrotron Diffraction of the Electrochemical Reduction Pathway of TiO₂, *Acta Mater.* 58 (2010) 5057–5062.
- [30] W. Xiao, X.B. Jin, Y. Deng, D.H. Wang, X.H. Hu, G.Z. Chen, Electrochemically Driven Three-Phase Interlines into Insulator Compounds: Electroreduction of Solid SiO₂ in Molten CaCl₂, *Chem. Phys. Chem.* 7 (2006) 1750–1758.
- [31] K. Jiang, X.H. Hu, M. Ma, D.H. Wang, G.H. Qiu, X.B. Jin, G.Z. Chen, Perovskitization-assisted Electrochemical Reduction of Solid TiO₂ in Molten CaCl₂, *Angew. Chem. Int. Ed.* 45 (2006) 428–432.
- [32] Q. Song, Q. Xu, X. Kang, J. Du, Z. Xi, Mechanistic Insight of Electrochemical Reduction of Ta₂O₅ to Tantalum in a Eutectic CaCl₂-NaCl Molten Salt, *J. Alloys Compd.* 490 (2010) 241–246.
- [33] T. Wu, X.B. Jin, W. Xiao, X.H. Hu, D.H. Wang, G.Z. Chen, Thin Pellets: Fast Electrochemical Preparation of Capacitor Tantalum Powder, *Chem. Mater.* 19 (2007) 153–160.
- [34] E. Gordo, G.Z. Chen, D.J. Fray, Toward Optimisation of Electrolytic Reduction of Solid Chromium Oxide to Chromium Powder in Molten Chloride Salts, *Electrochim. Acta* 49 (2004) 2195–2208.
- [35] D.T.L. Alexander, C. Schwandt, D.J. Fray, Microstructural Kinetics of Phase Transformations During Electrochemical Reduction of Titanium Dioxide in Molten Calcium Chloride, *Acta Mater.* 54 (2006) 2933–2944.
- [36] A.M. Abdelkader, D.J. Fray, Electro-deoxidation of Hafnium Dioxide and Niobia-doped Hafnium Dioxide in Molten Calcium Chloride, *Electrochim. Acta* 64 (2012) 10–16.
- [37] K.S. Mohandas, D.J. Fray, Electrochemical Deoxidation of Solid Zirconium Dioxide in Molten Calcium Chloride, *Metall. Mater. Trans. B* 40B (2009) 685–699.
- [38] C. Schwandt, D.T.L. Alexander, D.J. Fray, The Electro-deoxidation of Porous Titanium Dioxide Precursors in Molten Calcium Chloride under Cathodic Potential Control, *Electrochim. Acta* 54 (2009) 3819–3829.
- [39] D. Sri Maha Vishnu, N. Sanil, L. Shakila, G. Panneerselvam, R. Sudha, K.S. Mohandas, K. Nagarajan, A Study of the Reaction Pathways during Electrochemical Reduction of Dense Nb₂O₅ Pellets in molten CaCl₂ Medium, *Electrochim. Acta* 100 (2013) 51–62.
- [40] M.Я. ШПИИРТ, N. Zhang, Germanates and Silicon germanates, *Hydrometallurgy of China* 1 (1985) 50–56.
- [41] X.Y. Yan, D.J. Fray, Electrochemical Studies on Reduction of Solid Nb₂O₅ in Molten CaCl₂-NaCl Eutectic - I. Factors Affecting Electrodeoxidation of solid Nb₂O₅ to Niobium, *J. Electrochem. Soc.* 152 (2005) D12–D21.
- [42] D.J.S. Hyslop, A.M. Abdelkader, A. Cox, D.J. Fray, Electrochemical Synthesis of a Biomedically Important Co-Cr alloy, *Acta Mater.* 58 (2010) 3124–3130.
- [43] D.T.L. Alexander, C. Schwandt, D.J. Fray, The Electro-deoxidation of Dense Titanium Dioxide Precursors in Molten Calcium Chloride Giving a New Reaction Pathway, *Electrochim. Acta* 56 (2011) 3286–3295.
- [44] W. Li, X.B. Jin, F.L. Huang, G.Z. Chen, Metal-to-oxide Molar Volume Ratio: The Overlooked Barrier to Solid-state Electroreduction and a green Bypass Through Recyclable NH₄HCO₃, *Angew. Chem. Int. Ed.* 49 (2010) 3203–3206.
- [45] G.M. Haarberg, K.S. Osen, R.J. Heus, J.J. Egan, Electronic Conduction and Electron Mobilities in Molten NaCl-Na Solutions, *J. Electrochem. Soc.* 137 (1990) 1777–2781.
- [46] U. Stohr, W. Freyland, Intervalence Charge Transfer and Electronic Transport in Molten Salts Containing Tantalum and Niobium Complexes of Mixed Valency, *Phys. Chem. Chem. Phys.* 1 (1999) 4383–4387.